MIMO OTFS With Arbitrary Time-Frequency Allocation for Joint Radar and Communications

Correas Serrano, Aitor ; Petrov, Nikita; Gonzalez-Huici, Maria; Yarovoy, Alexander

DOI
10.1109/TRS.2023.3329918

Publication date
2023

Document Version
Final published version

Published in
IEEE Transactions on Radar Systems

MIMO OTFS With Arbitrary Time-Frequency Allocation for Joint Radar and Communications

Aitor Correas-Serrano, Nikita Petrov, Maria Gonzalez-Huici, and Alexander Yarovoy, *Fellow, IEEE*

***Abstract*— This paper proposes a novel waveform, namely non-uniform OTFS (NU-OTFS), for joint radar and communication applications (Radcom) in multi-user/MIMO scenarios. Based on orthogonal time frequency space (OTFS) modulation, the proposed waveform is realized by using a non-uniform symplectic finite Fourier transform (NU-SFFT) to generate non-overlapping quasi-arbitrary time-frequency representations of OTFS messages. Non-uniform sampling and sparse reconstruction algorithms within the compressed sensing framework are employed to avoid (self-)interference and enhance radar target parameter estimation. The performance of NU-OTFS and its corresponding receivers is evaluated through numerical simulations and measurements, and compared with state-of-the-art MU/MIMO Radcom OTFS system concepts. NU-OTFS allows for increased flexibility in time-frequency resource allocation and larger unambiguous radar parameter estimation while showing comparable performance to state-of-the-art OTFS multi-user communication implementations in realistic high-mobility channel conditions.**

***Index Terms*— Orthogonal time-frequency space (OTFS), multiple-input-multiple-output (MIMO), compressed sensing (CS), sparse reconstruction, radar-communication (Radcom), radar sensing.**

I. Introduction

THE advent of compact software-defined radar systems able to generate fully digital waveforms, together with the issue of the congested spectrum, has motivated research in systems able to perform joint communication and sensing (Radcom) tasks in the same frequency bands [1]. Radcom functionality has been investigated in a variety of forms, such as htrough embedding information in the sidelobes of a radar system [2], coexistence through array partitioning and waveform optimization [3], using index modulation exploiting the various degrees of freedom in radar systems [4], or leveraging beneficial frame structures of existing communication protocols to enable radar operation [5]. Another common approach to Radcom is the direct use of communication waveforms for radar, enabled by the development of fully digital radar systems [6]. In this context, multicarrier waveforms based on orthogonal frequency division multiplexing (OFDM) are promising in achieving good radar and communications performance without significant changes in existing communication system design [7], [8], [9]. Recently, orthogonal time-frequency space (OTFS) [10] modulation has gathered attention as an OFDM alternative for communications and radar in high-mobility scenarios [11]. Unlike OFDM, in which the symbols are defined over the time-frequency grid, OTFS symbols are defined over the "delay-Doppler" plane and spread over the time-frequency plane through the symplectic finite Fourier transform (SFFT). Higher Doppler tolerance [12], shorter cyclic prefix [13], and lower PAPR in typical usage scenarios [14] make this waveform a candidate for potential improvement over OFDM modulations for radar and Radcom. Recent studies show that OTFS can have comparable radar performance as OFDM, depending on the range-Doppler estimation approach [15].

Besides range and velocity, estimating the angular position of reflecting targets through array processing is crucial in many radar applications, such as automotive radar [7]. MIMO radar effectively increases the angular resolution with fewer array elements by exploiting path diversity between different transmit-receive pairs [16]. MIMO radar relies on the separability of the signals emitted by each transmitter to increase angular resolution [17]. In communications, signal separability from different transmitters is also required to enable simultaneous access for multiple users sharing the same bandwidth [18]. Therefore the ability to multiplex different radar transmitters or communication users such that they are separable in a receiver is desirable for both radar and communication applications. In OFDM, this can be accomplished by multiplexing the different transmitters directly in the time-frequency (TF) domain, allocating non-overlapping TF bins to different transmitters [18]. Under realistic channel conditions, the signal associated to different transmitters/users can be recovered by filtering the appropriate TF resource blocks in the receiver [19].

OTFS symbols are defined in the delay-Doppler (DD) domain and are later spread in the TF domain through the Inverse Symplectic Finite Fourier Transform (ISFFT). This causes the symbols to overlap in the TF domain, where different transmitters can not be separated anymore. Multiplexing directly on the DD domain is also not trivial, as time-frequency shifts in the channel result in a quasi-periodic 2D rotation of the symbols in this domain [20], and separating the transmitters without prior knowledge of the channel can

Manuscript received 14 July 2023; revised 27 September 2023 and 24 October 2023; accepted 30 October 2023. Date of publication 6 November 2023; date of current version 24 November 2023. *(Corresponding author: Aitor Correas-Serrano.)*

Aitor Correas-Serrano and Maria Gonzalez-Huici are with the Fraunhofer-Institut für Hochfrequenzphysik und Radartechnik (FHR), 53343 Wachtberg, Germany (e-mail: aitor.correas@fhr.fraunhofer.de).

Nikita Petrov is with NXP Semiconductors N.V., 5600 KA Eindhoven, The Netherlands, and also with the Department of Microelectronics, Faculty of Electrical Engineering, Mathematics and Computer Science, Delft University of Technology, 2628 CD Delft, The Netherlands.

Alexander Yarovoy is with the Department of Microelectronics, Faculty of Electrical Engineering, Mathematics and Computer Science, Delft University of Technology, 2628 CD Delft, The Netherlands.

Digital Object Identifier 10.1109/TRS.2023.3329918

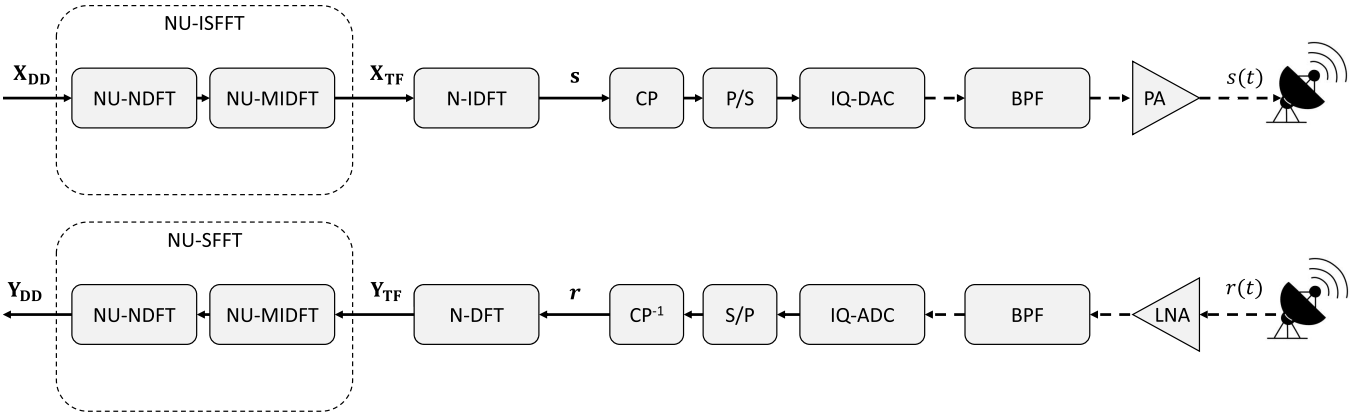

Fig. 1. Block diagram of a single channel NU-OTFS for MU/MIMO showing the non-uniform (NU) ISFFT operators. In transmit, the NU-ISFFT is implemented using a non-uniform DFT along the N dimension (NU-NDFT) and an inverse NU-DFT along the M dimension (NU-MIDFT). An IDFT along the N dimension (N-IDFT) is used to transform the time-frequency signal into a time domain signal. Transmission occurs after cyclic-prefix appending (CP), digital to analog conversion (DAC), band-pass filtering (BPF), and amplification (PA). The inverse operations are carried out in the receiver chain.

be difficult. It is possible to exploit channel characteristics, such as diversity in user mobility, to minimize inter-user interference [21], achieving improved performance for user multiplexing but not allowing for transmitter multiplexing in MIMO radar without channel knowledge. Specific DD resource allocations that allow for separability in the time-frequency domain have been studied in [22] and [23] for multiple user access for OTFS communications. The resulting TF representation amounts to interleaving or block allocation of transmitters/users in the TF resource plane. Such allocation is problematic for radar applications, as it reduces the non-ambiguous interval or resolution in either range or Doppler domain [24]. Alternative TF allocation schemes, particularly non-uniform optimized [25] or random patterns [24], have shown great promise in OFDM radar applications when paired with sparse reconstruction algorithms. Sparse reconstruction algorithms have shown potential in various aspects of radar signal processing [26] and interference mitigation [27] due to the inherent sparsity of radar data in the delay-Doppler-angle domain.

In this work, a novel waveform that maps an OTFS frame into quasi-arbitrary TF patterns is proposed, increasing the multiplexing flexibility of OTFS in both MIMO radar and MU communications. The proposed waveform is referred to as non-uniform OTFS (NU-OTFS). Specifically, the main contributions of this article are the following.

1) A generalized formulation for time-frequency multiplexing of OTFS signals, resulting in the NU-OTFS waveform. A non-uniform ISFFT (NU-ISFFT) is defined using non-uniform discrete Fourier operators for its implementation. The NU-ISFFT is used to generate non-overlapping TF representations of the OTFS messages and recover the OTFS message from a partially sampled TF plane. This non-overlapping representation enables transmitter/user separation at the receiver by filtering out the unwanted time-frequency samples in the digital domain. The inverse transform (NU-SFFT) is then used to move back to the original DD representation from the sparsely sampled TF signal. This formulation is general and can be used to include fixed patterns presented in previous work, such as interleaved TF allocation [23], as well as other quasi-arbitrary non-uniform patterns. Non-uniform time-frequency multiplexing is novel in OTFS waveforms. NU-OTFS could also simplify the implementation of high-bandwidth multistatic radar networks with reduced interference due to the increased flexibility in time-frequency resource allocation. A schematic depiction of the proposed scheme for transmission and reception is shown in Fig. 1.
2) A simulation and measurement-based evaluation of the performance of the proposed NU-OTFS waveform for monostatic MIMO radar applications. This is the first measurement-based OTFS radar validation reported in the literature, to the best of the author's knowledge. A signal processing chain based on compressed sensing (CS) is proposed, compared to traditional OTFS implementations, and validated through measurements.
3) A simulation-based study of the communications performance of NU-OTFS compared to other OTFS approaches, using standard 3GPP vehicular channel models [28] for simulation. A numerical comparison of error rates for different SNR and channel mobility values is drawn.

The remainder of the article is structured as follows. Section II presents a mathematical description of OTFS signal generation and channel effects and presents a novel system concept based on the NU-SFFT to generate the proposed NU-OTFS waveform. Section III includes descriptions of NU-OTFS radar and communication receivers. Section IV presents numerical radar and communications performance simulations for the proposed NU-OTFS system concept, as well as experimental validation for NU-OTFS radar. Finally, concluding remarks are given in section V.

Notation: Throughout this article, $\mathbf{A}^{\mathrm{H}}$ and $\mathbf{A}^{-1}$ denote the conjugate transpose and inverse of the matrix $\mathbf{A}$ respectively; $\mathrm{vec}(\mathbf{A})$ turns the $N \times M$ matrix $\mathbf{A}$ into a $NM \times 1$ vector $\mathbf{a}$, and $\mathrm{vec}(\mathbf{a})^{-1}_{N\times M}$ is the inverse operation; $\mathrm{diag}(\mathbf{b})$ turns the $N \times 1$ vector $\mathbf{b}$ into a $N \times N$ diagonal matrix $\mathbf{B}$ whose main diagonal is $\mathbf{b}$. Finally, $\odot$ represents the matrix element-wise (Hadamard) product.

II. OTFS Signal Model

Consider a single transmitter OTFS system transmitting a message $\mathbf{X}_{\mathrm{DD}} \in \mathbb{C}^{N\times M}$ defined in a $N \times M$ delay-Doppler grid, with N delay bins and M Doppler bins. The number of

subcarriers and subsymbols in TF representation is N and M, respectively. The communication symbols are mapped to the time-frequency domain through the inverse symplectic Fourier transform (ISFFT) such that

$$\mathbf{X}_{\mathrm{TF}}[n,m] = \frac{1}{\sqrt{NM}} \sum_{k=0}^{N-1} \sum_{l=0}^{M-1} \mathbf{X}_{\mathrm{DD}}[k,l] e^{j2\pi\left(\frac{nk}{N} - \frac{ml}{M}\right)} \quad (1)$$

where $[k,l]$ are index pairs in the delay-Doppler grid, and $[n,m]$ are index pairs in the time-frequency grid. $\mathbf{X}_{\mathrm{TF}}[n,m]$ is the time-frequency representation of the OTFS symbols, now spread in the time-frequency domain. The TF signal is converted into the time domain for transmission using the Heisenberg transform. The time domain signal $s(t)$ is given by

$$s(t) = \sum_{n=0}^{N-1} \sum_{m=0}^{M-1} \mathbf{X}_{\mathrm{TF}}[n,m] g_{tx}(t-nT) e^{j2\pi m \Delta \mathrm{f}(t-nT)} \quad (2)$$

where g_{tx} is the transmit pulse. Assuming a rectangular transmit pulse and a critically sampled signal, equations (1) and (2) can be written in compact matrix notation as

$$\mathbf{X}_{\mathrm{TF}} = \mathbf{F}_{\mathrm{N}} \mathbf{X}_{\mathrm{DD}} \mathbf{F}_{\mathrm{M}}^{\mathrm{H}} \quad (3)$$

and

$$\mathbf{s} = \mathrm{vec}\left(\mathbf{F}_{\mathrm{N}}^{\mathrm{H}} \mathbf{X}_{\mathrm{TF}}\right) = \mathrm{vec}\left(\mathbf{X}_{\mathrm{DD}} \mathbf{F}_{\mathrm{M}}^{\mathrm{H}}\right) \quad (4)$$

where $\mathbf{F}_{\mathrm{N}} \in \mathbb{C}^{N\times N}$ and $\mathbf{F}_{\mathrm{M}} \in \mathbb{C}^{M\times M}$ are normalized Fourier transform matrices. The discrete time-domain signal $\mathbf{s} \in \mathbb{C}^{NM\times 1}$ is transformed to the analog domain with a digital-to-analog converter (DAC) before undergoing I/Q modulation to the desired carrier frequency f_c. For this work, narrowband signals are assumed in all steps, and therefore, $f_c \gg B$, where $B = N\Delta \mathrm{f}$ is the bandwidth of the OTFS signal. In both communication and radar applications, the received signal is a linear combination of multiple time and frequency-shifted replicas of the transmitted signal embedded in noise. For a single point target, and after undergoing I/Q demodulation and sampling, it can be written compactly as

$$\mathbf{r} = \mu\psi \mathrm{vec}(\mathbf{\Gamma_1} \mathbf{F}_{\mathrm{N}}^{\mathbf{H}} \mathbf{A} \mathbf{X}_{\mathrm{TF}} \mathbf{\Gamma_2}) \quad (5)$$

where, for a delay τ and a Doppler shift f_d, the following constants are defined

$$\gamma = \exp\left(-j2\pi \frac{T}{N} f_d\right) \quad (6)$$

$$a = \exp(-j2\pi \Delta f \tau) \quad (7)$$

and used to build diagonal matrices modeling the time and frequency shift in the received signal:

$$\mathbf{\Gamma}_1 = \mathrm{diag}\{\gamma^0, \gamma^1, \ldots, \gamma^{(N-1)}\} \quad (8)$$

$$\mathbf{\Gamma}_2 = \mathrm{diag}\{\gamma^0, \gamma^N, \ldots, \gamma^{(M-1)N}\} \quad (9)$$

where $\mathbf{\Gamma}_1 \in \mathbb{C}^{N\times N}$ represents the Doppler phase shift along subcarriers - the intercarrier interference - and $\mathbf{\Gamma}_2 \in \mathbb{C}^{M\times M}$ is the Doppler phase shift across subpulses. Analogously, a matrix form of the target range-related subcarrier phase shift is defined as

$$\mathbf{A} = \mathrm{diag}\{a^0, a^1, \ldots, a^{N-1}\} \quad (10)$$

with $\mathbf{A} \in \mathbb{C}^{N\times N}$. Finally, μ is a complex amplitude, and ψ represents the delay-dependent phase shift at carrier frequency

$$\psi = \exp(-j2\pi f_c \tau) \quad (11)$$

Equations (1), (4), and (5) describe the generation of the transmitted and received time-domain signal in a single-transmitter OTFS system, where the entirety of the available time-frequency resources are used by a single radar transmitter or communications user.

A. NU-OTFS Transmitter Multiplexing

For an extension to MU/MIMO case, the signals originating from different users/transmitters must be separable at the receiver. Let us consider the critically sampled received signal in (5), then the time-frequency representation of the received target response is given by

$$\mathbf{Y}_{\mathrm{TF}} = \mathbf{F}_{\mathrm{N}} \mathrm{vec}_{N\times M}^{-1}(\mathbf{r}) \quad (12)$$

and the delay-Doppler received signal is given by

$$\mathbf{Y}_{\mathrm{DD}} = \mathbf{F}_{\mathrm{N}}^{\mathrm{H}} \mathbf{Y}_{\mathrm{TF}} \mathbf{F}_{\mathrm{M}} \quad (13)$$

which can also be written in the discrete delay-Doppler domain as [20]

$$y_{\mathrm{DD}}[k',l'] = \sum_{k'=0}^{N-1} \sum_{l'=0}^{M-1} h[k',l'] \exp\left(j\frac{2\pi}{NM}[l-l']_M[k']_N\right) \times \alpha[k,l] x[[k-k']_N, [l-l']_M] \quad (14)$$

where

$$\alpha[k,l] = \begin{cases} 1 & \text{if } l' \le l < M \\ \exp\left(-j2\pi \frac{k}{N}\right) & \text{if } 0 \le l < l' \end{cases} \quad (15)$$

where $[\cdot]_N$ and $[\cdot]_M$ denote modulo N and M operations respectively. This notation highlights the effect of targets with amplitude $h[k',l']$, delay k' and Doppler shift l' on the received signal, that appear as circular shifts of the transmitted symbols in the delay-Doppler domain. Due to this shift in the delay-Doppler representation, different communication users or radar transmitters can not be separated easily in the delay-Doppler domain without prior channel knowledge. Alternatively, the signal associated with different transmitters can be identified if non-overlapping sets of time-frequency bins are assigned to each of them. This approach is common in MU/MIMO OFDM applications [18].

In OTFS, the DD symbols are spread in the TF domain after the ISFFT in (1) and (3), therefore non-overlapping DD signals can overlap in the TF domain. Some specific arrangements of DD symbols studied in the literature, such as block division or interleaving in the DD domain, result in an interleaving or block division respectively in the time-frequency domain [23]. These arrangements are specific forms of the common time-division (symbol) or frequency-division (subcarrier) multiplexing in MU/MIMO OFDM. Fig. 2a shows a delay-Doppler multiplexing of two transmitters that, when represented in the time-frequency domain through the

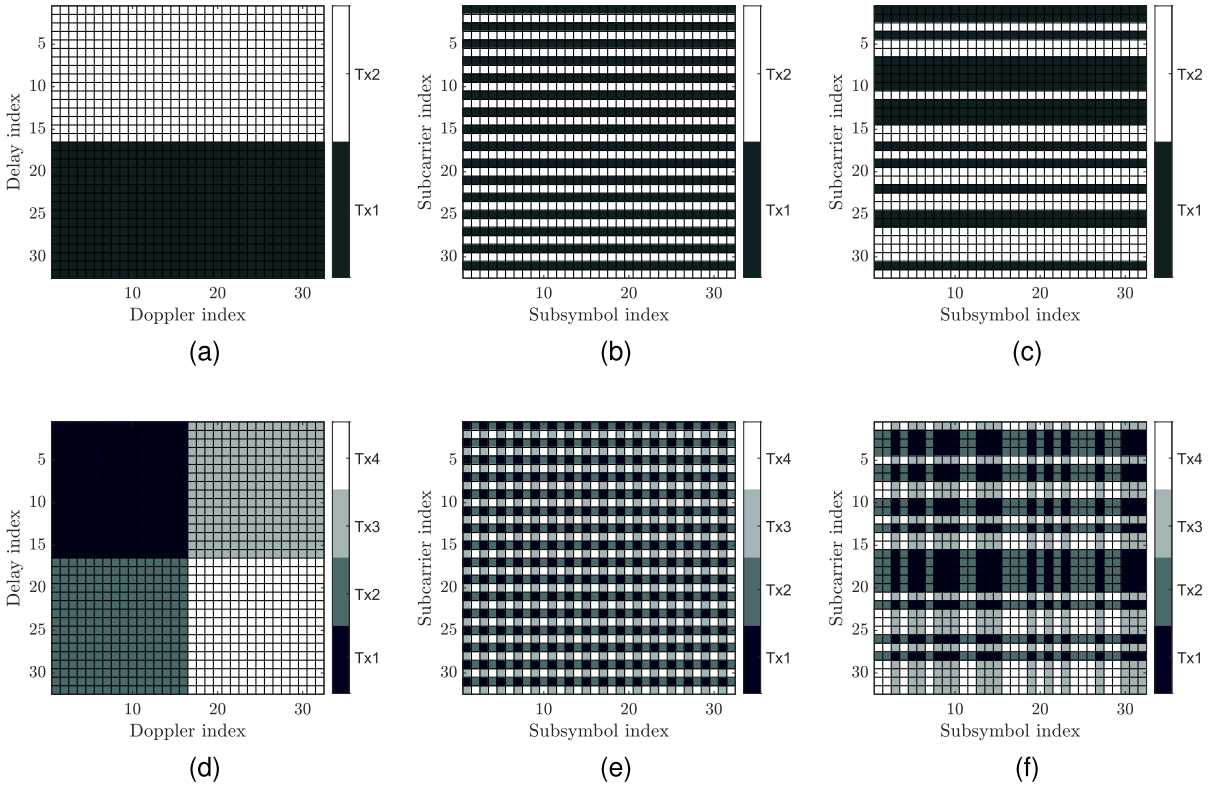

Fig. 2. Depiction of multiplexing strategy in delay-Doppler representation, standard interleaved multiplexing in time-frequency, and quasi-arbitrary multiplexing in time-frequency with NU-OTFS. (a) delay-Doppler representation of two multiplexed waveforms; (b) interleaved multiplexing in the TF domain; (c) arbitrary multiplexing across subcarriers in the TF domain with NU-OTFS. For 2D quasi-arbitrary multiplexing: (d) four transmitters multiplexed in the delay-Doppler domain; (e) interleaved 2D multiplexing in the time-frequency domain; (f) quasi-arbitrary 2D multiplexing in the TF domain with NU-OTFS.

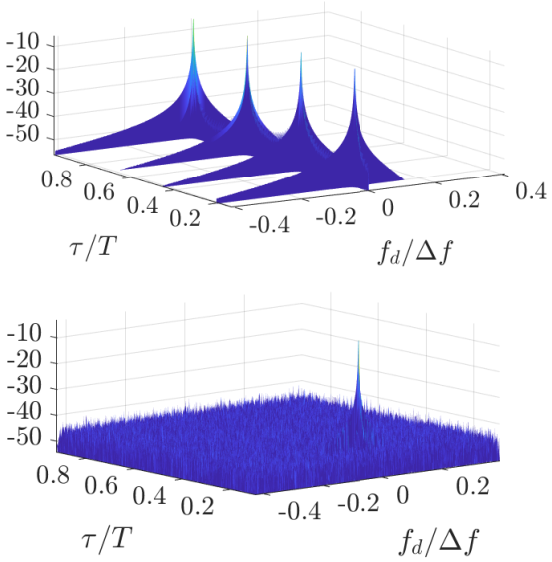

Fig. 3. Comparison of noiseless range-Doppler estimation with different MIMO approaches with four transmitters. On the top, subcarrier interleaving causes a reduction in the maximum unambiguous range. On the bottom, random multiplexing reduces the dynamic range of the estimation.

standard ISFFT, correspond to subcarrier interleaving (see Fig. 2b). This can be extended to 2D interleaved multiplexing, as seen in Figs. 2d and 2e. However, interleaved frequency and time multiplexing reduce the non-ambiguous range and Doppler respectively, as depicted in Fig. 3. To maintain the total range-Doppler unambiguous interval and transmitter separability in the TF domain, random TF multiplexing is a common approach for OFDM radar. To accomplish quasi-arbitrary time-frequency multiplexing for OTFS signals, a non-uniform ISFFT (NU-ISFFT) can be defined by using non-uniform discrete Fourier transform (DFT) operators.

First, let $\mathbf{X}_{\mathrm{DD}}^{\mathrm{MIMO}}$ be defined as

$$\mathbf{X}_{\mathrm{DD}}^{\mathrm{MIMO}} = \begin{bmatrix} \mathbf{X}_{\mathrm{DD}}^{(1,1)} & \cdots & \mathbf{X}_{\mathrm{DD}}^{(1,\sqrt{N_{\mathrm{Tx}}})} \\ \vdots & \ddots & \vdots \\ \mathbf{X}_{\mathrm{DD}}^{(\sqrt{N_{\mathrm{Tx}}},1)} & \cdots & \mathbf{X}_{\mathrm{DD}}^{(\sqrt{N_{\mathrm{Tx}}},\sqrt{N_{\mathrm{Tx}}})} \end{bmatrix} \tag{16}$$

where $\mathbf{X}_{\mathrm{DD}}^{(p,q)} \in \mathbb{C}^{(N/\sqrt{N_{\mathrm{Tx}}})\times(M/\sqrt{N_{\mathrm{Tx}}})}$ are the delay-Doppler messages associated to different transmitters, and $\mathbf{X}_{\mathrm{DD}}^{\mathrm{MIMO}} \in \mathbb{C}^{N\times M}$ is the OTFS MIMO frame for a monostatic OTFS radar with N_{Tx} transmitters. For simplicity of notation, it is assumed that N_{Tx} is a square number to assume equal distribution of the messages in the delay and Doppler domain. This is not a necessary condition, as any non-prime number of transmitters can be distributed in tiles across the delay-Doppler domain, or some time-frequency resources can be left unoccupied. Equation (3) can be altered to design a mapping between $\mathbf{X}_{\mathrm{DD}}$ and a TF representation with a quasi-arbitrary TF occupancy pattern. This mapping is denoted here as the NU-ISFFT. For transmitter n_{Tx}, let $\boldsymbol{\xi}_{N,n_{\mathrm{Tx}}} \in \{0,1\}^{N\times 1}$ be a vector indexing the active subcarriers, $\boldsymbol{\xi}_{M,n_{\mathrm{Tx}}} \in \{0,1\}^{M\times 1}$ a vector indexing the active time subsymbols, $\boldsymbol{\Xi}_N^{(n_{\mathrm{Tx}})} = \mathrm{diag}\{\boldsymbol{\xi}_{N,n_{\mathrm{Tx}}}\}$, and $\boldsymbol{\Xi}_M^{(n_{\mathrm{Tx}})} = \mathrm{diag}\{\boldsymbol{\xi}_{M,n_{\mathrm{Tx}}}\}$, then

$$\mathbf{X}_{\mathrm{TF}}^{(n_{\mathrm{Tx}})} = \boldsymbol{\Xi}_N^{(n_{\mathrm{Tx}})}\mathbf{F}_N\mathbf{X}_{\mathrm{DD}}^{(n_{\mathrm{Tx}})}\mathbf{F}_M^{\mathrm{H}}\boldsymbol{\Xi}_M^{(n_{\mathrm{Tx}})} \tag{17}$$

$$\mathbf{X}_{\mathrm{TF}}^{\mathrm{MIMO}} = \sum_{n_{tx}=1}^{N_{\mathrm{Tx}}} \mathbf{X}_{\mathrm{TF}}^{(n_{\mathrm{Tx}})} \tag{18}$$

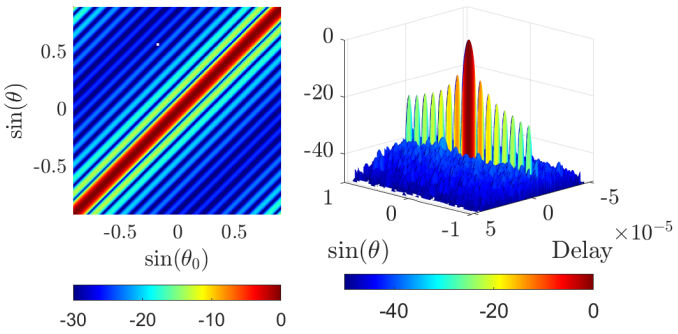

Fig. 4. MIMO radar ambiguity function (AF) for NU-OTFS, with 16 transmitters and $N = 1024$, $M = 512$. On the left, the angular AF shows that the angular spectrum is constant regardless of the target's angular position. On the right, the range-angle AF shows no artifacts or ambiguities in the delay estimation for the entire signal length.

where $\mathbf{X}_{\mathrm{TF}}^{(n_{\mathrm{Tx}})} \in \mathbb{C}^{N\times M}$ is the sparse time-frequency representation of the signal associated to the n_{Tx}-th transmitter, and $\mathbf{X}_{\mathrm{TF}}^{\mathrm{MIMO}} \in \mathbb{C}^{N\times M}$ is the time-frequency representation of all the transmitters. In order to achieve arbitrary non-overlapping time representations, it is necessary that

$$\left(\boldsymbol{\xi}_{N,n_{\mathrm{Tx}}}\boldsymbol{\xi}_{M,n_{\mathrm{Tx}}}^{T}\right)\odot\left(\boldsymbol{\xi}_{N,n'_{\mathrm{Tx}}}\boldsymbol{\xi}_{M,n'_{\mathrm{Tx}}}^{T}\right)=\mathbf{0}\quad\forall\quad n_{\mathrm{Tx}}\neq n'_{\mathrm{Tx}}\tag{19}$$

where $\mathbf{0}$ is the $N\times M$ all zero matrix. Equation (19) forces that no pair of subcarrier-subsymbol is occupied by more than one transmitter. Uniform sampling is performed in the subsymbol dimension if $\boldsymbol{\Xi}_M = \mathbf{I}$, and in the subcarrier if $\boldsymbol{\Xi}_N = \mathbf{I}$. The TF patterns arising from the NU-ISFFT are not truly arbitrary, but rather the intersections of two one-dimensional arbitrary assignations of time and subcarrier resources defined by $\boldsymbol{\xi}_{M,n_{\mathrm{Tx}}}$ and $\boldsymbol{\xi}_{N,n_{\mathrm{Tx}}}$ respectively. The proposed multiplexing is depicted in Fig. 2c for multiplexing across the delay/frequency domain and Fig. 2f for multiplexing across both the delay/frequency and Doppler/time domain.

Finally, the transmitted time-domain signal is obtained by applying the standard Heisenberg transform to the new TF signal representation, substituting (18) in (4),

$$\mathbf{s}^{\mathrm{MIMO}}=\mathrm{vec}\left(\mathbf{F}_{\mathrm{N}}^{\mathrm{H}}\mathbf{X}_{\mathrm{TF}}^{\mathrm{MIMO}}\right)\tag{20}$$

The MIMO transmit ambiguity function (AF) (as defined in e.g., [29]) of the signal in (20) is shown in Fig. 4. The MIMO AF shows constant amplitude regardless of target position and no ambiguities or abnormal sidelobes in the range-angular cut, showing no angle-dependent interference between transmitters.

III. NU-OTFS Receiver

A. NU-OTFS MIMO Radar Receiver

Consider a critically sampled received echo from a point target at relative azimuth angle ϕ, in an NU-OTFS MIMO system with N_{Tx} transmitters and N_{Rx} receivers arranged in a one-dimensional array, with their positions given by $\mathbf{d}_{\mathrm{Tx}} \in \mathbb{R}^{N_{\mathrm{Tx}}\times 1}$ and $\mathbf{d}_{\mathrm{Rx}} \in \mathbb{R}^{N_{\mathrm{Rx}}\times 1}$ respectively. The steering vector

$$\mathbf{a}(\phi):=\exp\left(j\frac{2\pi}{\lambda}\mathbf{d}_{\mathrm{Tx}}\sin(\phi)\right)\tag{21}$$

with $\mathbf{a}(\phi) \in \mathbb{C}^{N_{\mathrm{Tx}}\times 1}$ captures the direction-of-arrival dependent phase shift associated to the position of the transmitters. Analogously, the angle-dependent phase shift at each receiver is given by

$$\mathbf{b}(\phi):=\exp\left(j\frac{2\pi}{\lambda}\mathbf{d}_{Rx}\sin(\phi)\right).\tag{22}$$

with $\mathbf{b}(\phi) \in \mathbb{C}^{N_{\mathrm{Rx}}\times 1}$. Then the received signal at receiver n_{Rx} can be written as

$$\mathbf{r}_{n_{\mathrm{Rx}}}^{\mathrm{MIMO}}=\mu\psi b_{n_{\mathrm{Rx}}}(\phi)\sum_{n_{\mathrm{Tx}}=1}^{N_{\mathrm{Tx}}}a_{n_{\mathrm{Tx}}}(\phi)\mathrm{vec}\left(\boldsymbol{\Gamma}_1\mathbf{F}_{\mathrm{N}}^{\mathbf{H}}\mathbf{A}\mathbf{X}_{\mathrm{TF}}^{\mathrm{MIMO}}\boldsymbol{\Gamma}_2\right)\tag{23}$$

where n_{Tx} and n_{Rx} denote the transmitter and receiver index respectively, and $a_{n_{\mathrm{Tx}}}$ and $b_{n_{\mathrm{Rx}}}$ denote the steering vector entry associated with this index. Co-located MIMO and far-field targets are assumed, and therefore the delay and Doppler shifts associated to each transmit-receive pair are considered the same.

Similarly to (12), the TF representation of the signal at receiver n_{Rx} is given by

$$\mathbf{Y}_{\mathrm{TF},n_{\mathrm{Rx}}}^{\mathrm{MIMO}}=\mathbf{F}_{\mathrm{N}}\mathrm{vec}_{N\times M}^{-1}(\mathbf{r}_{n_{\mathrm{Rx}}}^{\mathrm{MIMO}})\tag{24}$$

Henceforth, a single receiver is assumed and the n_{Rx} suffix is omitted to simplify notation. This can be done without loss of generality, as the process of receiving and separating the different transmit signals is invariant to the number of receivers. Each transmitted signal can now be separated in the receiver by

$$\mathbf{Y}_{\mathrm{TF}}^{(n_{\mathrm{Tx}})}=\boldsymbol{\Xi}_N^{(n_{\mathrm{Tx}})}\mathbf{Y}_{\mathrm{TF}}^{\mathrm{MIMO}}\boldsymbol{\Xi}_M^{(n_{\mathrm{Tx}})}\tag{25}$$

thus retrieving the signal associated to the n_{Tx} transmitter, and completing the MIMO implementation of NU-OTFS. Further steps involve the range-Doppler estimation in each transmit-receive pair.

Regarding OTFS radar receivers, multiple options have been proposed in the literature. A matched filter in the delay-Doppler domain is described in [30] and [31], which accomplishes high Doppler tolerance. However, it involves joint estimation of range and Doppler, making its computational complexity prohibitive for typical radar applications. Therefore, a radar receiver based on a spectral division in the time-frequency domain [15] is chosen as an alternative. Although the chosen receiver degrades for high Doppler shifts, its computation involves only DFT processing to effectively transform the spectral-normalized TF representation of the received signal into the estimation domain. The implementation involves only the SFFT processing and a symbol-wise division, and the range and Doppler estimations are assumed to be decoupled. This estimation approach can be used together with non-uniform subcarrier multiplexing to maintain the full unambiguous range estimation. Doppler compensating approaches such as all-cell Doppler correction (ACDC) [32] can be adapted to OTFS and used to exploit the increased maximum unambiguous Doppler resulting from non-uniform multiplexing in the time (subsymbol) domain. Further comparison between OTFS radar receivers can be found in [15].

In order to implement the spectral-division-based receiver [33], the TF representation of the received signal is

normalized with respect to the transmitted TF representation

$$\mathbf{Y}_{\text{div}}^{n_{\text{tx}}}[n,m] = \frac{\mathbf{Y}_{\text{TF}}^{n_{\text{tx}}}[n,m]}{\mathbf{X}_{\text{TF}}^{n_{\text{tx}}}[n,m]}, \tag{26}$$

for every $[n, m]$ that fulfills $\mathbf{X}_{\text{TF}}^{n_{\text{tx}}}[n,m] \neq 0$. After spectral division, an IDFT is performed over the columns and a DFT over the rows. This is the symplectic finite Fourier transform (SFFT), i.e. the transform shown in (13). This receiver normalizes the received signal in the time-frequency domain and transforms the result into the delay-Doppler domain. If $[\tau, f_d] = [0, 0]$, $\mathbf{Y}_{\text{div}}$ is an all-ones matrix, and its delay-Doppler representation $\mathbf{Y}_{\text{div}}^{\text{DD}}$ appears as a peak in $[0, 0]$. For any other pair of $[\tau_p, \upsilon_p]$, the peak in $\mathbf{Y}_{\text{div}}^{\text{DD}}$ is displaced to the corresponding index in the delay-Doppler plane.

B. Orthogonal Matching Pursuit (OMP)

Sparse reconstruction algorithms from Compressed Sensing (CS) are commonly used to mitigate the loss in dynamic range when non-uniform sampling is used [34]. A wide variety of algorithms with different performance and computational complexity have been proposed in the literature. For the radar simulations in this article, the Orthogonal Matching Pursuit (OMP) [35] algorithm is chosen, as it has shown good performance in automotive radar scenarios [36], [37], [38], [39], while being one of the least computationally expensive algorithms described in the CS literature. For more information on the experimental comparison of OMP with other sparse reconstruction algorithms in terms of computational complexity and performance, we refer the reader to [36]. OMP is a greedy iterative algorithm that does not require accurate knowledge of the number of targets in the scene. For N range or M Doppler hypotheses, OMP estimates the matched filter response in each channel as MF $:= \mathbf{A}^{\text{H}}\mathbf{r}_{i-1}$, where i is the iteration index, and $\mathbf{r}_0 = \mathbf{y}$. The sensing matrix for range and Doppler estimation are defined as $\mathbf{A}_\tau = [\mathbf{a}^{\text{T}}(\tau_1), \ldots, \mathbf{a}^{\text{T}}(\tau_N)]$ and $\mathbf{A}_\nu = [\mathbf{a}^{\text{T}}(\nu_1), \ldots, \mathbf{a}^{\text{T}}(\nu_M)]$ respectively, with

$$\mathbf{a}(\tau) := \exp\left(j\ 2\pi\,\Delta\text{f}\boldsymbol{\alpha}\frac{2r}{c_0}\right) \tag{27}$$

$$\mathbf{a}(\nu) := \exp\left(j\ 2\pi T\boldsymbol{\beta}\frac{\text{v}\,f_c}{c_0}\right) \tag{28}$$

where for a given transmitter, $\boldsymbol{\alpha}$ and $\boldsymbol{\beta}$ are vectors indexing the active subcarriers and subsymbols, respectively, and τ and ν represent the delay and Doppler shift hypotheses. For either range or Doppler estimation, the hypothesis n with the highest model match is selected

$$k_{\text{it}} := \arg\ \max_{n}\ \mathbf{A}^{\text{H}}\mathbf{r}_{\text{it}-1}. \tag{29}$$

A partial sensing matrix is built in each iteration with the hypotheses ψ_{it} of $\mathbf{A}$ selected in the current and previous iterations, such that $\Psi = [a_{\psi_1}, \ldots, a_{\psi_{\text{it}}}]$. The current estimate is calculated as

$$\hat{\mathbf{x}} = \Psi^{-1}\mathbf{y}. \tag{30}$$

the residual for the next iteration is $\mathbf{r}_{\text{it}+1} = \mathbf{y} - \hat{\mathbf{y}}$, where $\hat{\mathbf{y}} = \Psi\hat{\mathbf{x}}$. If stopping criteria are not met, the algorithm iterates back to (29). A stopping condition is usually defined as the residual power variation or a fixed number of iterations. The complexity of the algorithm grows linearly with the number of iterations and the dimensions of the sensing matrix. Therefore, for $\mathbf{A} \in \mathbb{C}^{P\times Q}$ and k iterations the complexity is $O(kPQ)$.

For radar data, it is possible to apply OMP for only range or Doppler estimation, or sequentially for both. The following approaches to range-Doppler estimation are defined for the sake of clarity.

- **2D-DFT:** The range-Doppler map is calculated through standard IDFT processing along subcarriers, and DFT along the subsymbols. Zero-filling is used for the subcarrier-subsymbol pairs not occupied by the selected transmitter.
- **Hybrid-OMP:** First, the Doppler estimation is performed through standard DFT processing, followed by range estimation with OMP using $\mathbf{A}_\tau$ as sensing matrix. This approach is aimed to minimize sidelobes in the range dimension, where bright targets near the radar could mask far away targets.
- **2D-OMP:** Range and Doppler estimations are performed sequentially with OMP. The range estimation uses $\mathbf{A}_\tau$ as sensing matrix, whereas the Doppler estimation uses $\mathbf{A}_\nu$. The approach offers the benefits of OMP in both range and Doppler dimensions.

C. NU-OTFS Multiuser Communications Receiver

One of the key advantages of the proposed NU-OTFS is increased flexibility in time-frequency allocation when multiplexing multiple communication users or when operating in a crowded spectrum. When it comes to OTFS communication receivers, multiple approaches have been proposed, such as the single-tap equalized, the LMMSE receiver [40] and a message passing algorithm receiver [41]. In this work, a standard LMMSE [42] receiver is used to validate the communications performance of the proposed NU-OTFS. The LMMSE receiver is more Doppler tolerant than the single-tap equalized receiver, and its adaptation to NU-OTFS frames is relatively straightforward. Although the computational complexity is $O(N^3M^3)$, implementations exploiting channel sparsity in the delay-Doppler domain with $O(\frac{MN}{2}\log_2 N)$ complexity have been proposed in [40]. Perfect knowledge of the channel $\mathbf{H}$ is assumed, as channel estimation approaches are not considered in the scope of this work. Assuming a noise variance σ_w^2, the LMMSE estimate of $\mathbf{X}_{\text{DD}}$ is given as

$$\hat{\mathbf{X}}_{\text{DD}}^{(n_{tx})} = (\mathbf{H}^{\text{H}}\mathbf{H} + \sigma_w^2\mathbf{I}_{\text{MN}})^{-1}\mathbf{H}^{\text{H}}\mathbf{Y}_{\text{DD}}^{(n_{tx})} \tag{31}$$

where $\mathbf{I}_{\text{MN}}$ is the identity matrix of size $MN \times MN$, and $\mathbf{H} \in \mathbb{C}^{NM\times NM}$ is the delay-Doppler channel matrix with as many non-zero elements in each row as discrete delay-Doppler paths in the channel. The received signal from the n_{Tx} user Y_{DD} is retrieved by applying the inverse of the transform in (17), that is, the NU-SFFT given by

$$\mathbf{Y}_{\text{DD}}^{(n_{tx})} = \boldsymbol{\Xi}_N^{(n_{tx})}\mathbf{F}_N^{\text{H}}\mathbf{X}_{\text{DD}}^{(n_{\text{tx}})}\mathbf{F}_M\,\boldsymbol{\Xi}_M^{(n_{tx})} \tag{32}$$

More information about the structure of the delay-Doppler channel matrix and the implementation of the LMMSE receiver for OTFS can be found in e.g. [42].

TABLE I
OTFS SIMULATIONS WAVEFORM PARAMETERS

Parameter	Symbol	Value
Number of delay bins	N	1024
Number of Doppler bins	M	512
Bandwidth	B	1 GHz
Carrier frequency	f_c	77 GHz
Symbol duration	T	1.02 μs
Intercarrier separation	Δf	977 kHz
Cyclic prefix duration	T_{cp}	1 μs
Communication Modulation	$(-)$	QPSK

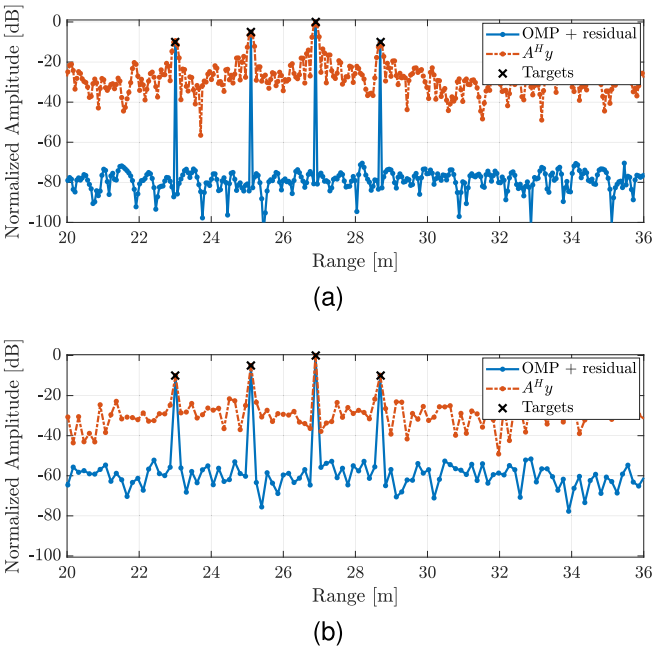

Fig. 5. Range cuts (a) on-grid targets and grid size of $3N$, and (b) off-grid targets and grid size of N. Signal to noise ratio is set to 20 dB.

IV. PERFORMANCE ASSESSMENT OF NU-OTFS

In this section, a series of numerical simulations are performed to validate the viability of NU-OTFS for radar and communications.

A. MIMO-OTFS Radar Performance Evaluation

In this section, a numerical analysis of NU-OTFS radar performance under the proposed MIMO configuration is performed. As OTFS is particularly well suited to communications in high mobility channels [43], the radar study is aimed at automotive applications, where high Doppler shifts are common and Radcom applications are gaining popularity. The waveform parameters displayed in Table I are chosen to match the standards in automotive applications (e.g., [6]).

The performance of the standard DFT-based spectral-division-based receiver is compared to an implementation of the same receiver using OMP as a solver. While OMP is a low-complexity algorithm, its performance in radar estimation is tied to its ability to detect and remove high-power targets accurately. Fig. 5 shows the dynamic range gain from using OMP in comparison to the straight correlation of the model $\mathbf{A}$ with the received signal $\mathbf{y}$ (equivalent to standard DFT processing, as $\mathbf{A}$ is a non-uniform DFT matrix). The full potential of the algorithm can be seen in Fig. 5a, showing an

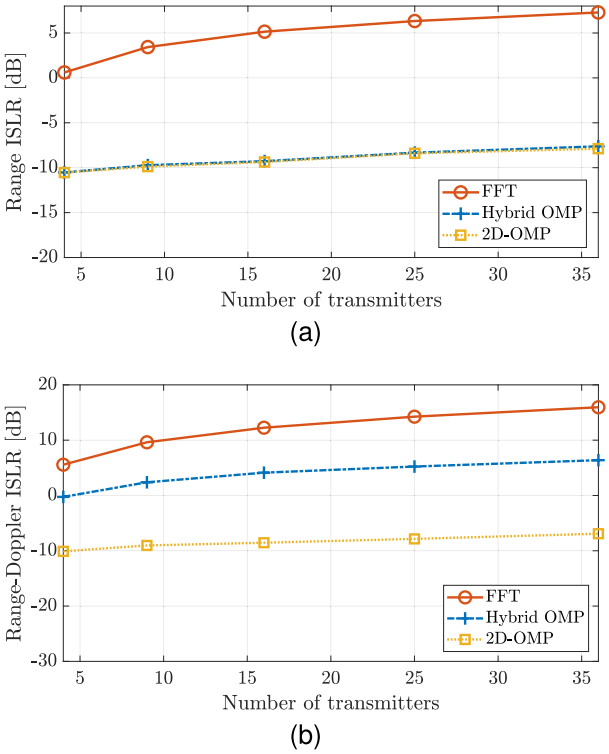

Fig. 6. ISLR for increasing number of transmitters and different estimation algorithm. (a) ISLR in the range cut; (b) ISLR of the entire range-Doppler surface.

improvement of around 60 dB when a very fine grid is used in the estimation, and the targets are defined on it. For a more practical scenario, with off-grid targets and a grid size of N, the dynamic-range improvement for the proposed scenario is around 30 dB, as shown in Fig. 5b. Specifically, a grid size of N for range estimation and M for Doppler estimation is used, with targets defined off-grid. Scenarios in Fig. 5 are simulated with SNR $=$ 20 dB.

Fig. 6 shows the integrated sidelobe ratio (ISLR) change in a scene with one target as the number of multiplexed transmitters increases. The ISLR is defined as the ratio between the power in the main lobe of the estimation and the integrated power of the sidelobes [44]. As the number of transmitters increases, the sparsity level in the estimation of range and Doppler in each channel increases accordingly. While this causes the ISLR to increase with the number of transmitters for all approaches, there is a 10 dB gain in range-Doppler ISLR when OMP processing is performed in the range dimension (hybrid-OMP), and up to 20 dB when OMP is used to sequentially estimate both range and Doppler (2D-OMP). Moreover, OMP-based approaches degrade visibly slower as the number of transmitters increases. A more visual appreciation of the improvement in sidelobe level can be seen in Fig. 7, where a section of the range-Doppler map with four targets shows that the hybrid-OMP (center) and 2D-OMP (right) have progressively lower sidelobes in both range and Doppler when compared with the DFT processing (left).

The spatial spectrum in a simulated system with multiple transmitters and one receiver (MISO) is compared to the spatial spectrum of a SIMO system with one transmitter and multiple receivers to validate the proposed MIMO

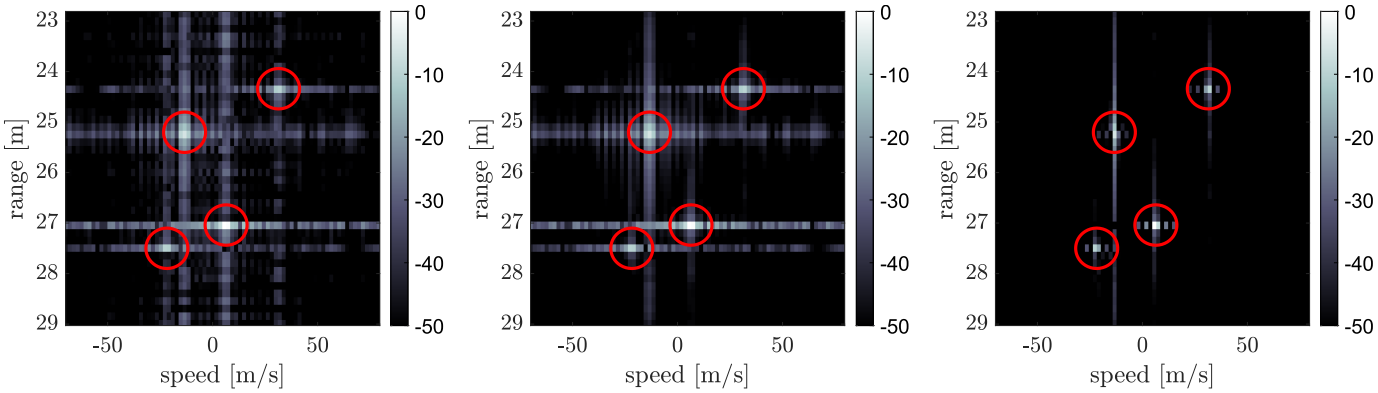

Fig. 7. Range-Doppler estimation of a single channel of sparse NU-OTFS waveform with four transmitters (i.e., sparsity rate of 25%). On the left, 2D-FFT processing. On the center, hybrid OMP estimation. On the right, 2D OMP.

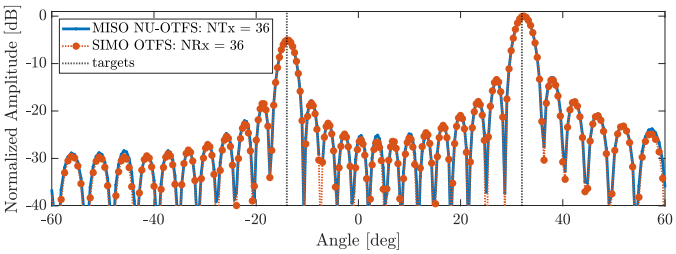

Fig. 8. Angular estimation of two targets. Comparison between NU-OTFS MISO case with 36 transmitters and one receiver, and standard OTFS SIMO case with one transmitter and 36 receivers. Good matching indicates orthogonality between transmitters in the proposed NU-OTFS waveform.

Fig. 9. Measured static target: Industrial chimney situated 1185 meters away from the sensor.

implementation. In both cases, the equivalent virtual arrays are uniformly spaced at $\lambda/2$ distance, and the spatial spectrum is computed using a discrete Fourier transform over the elements. The comparison is shown in Fig. 8, where the MISO result closely resembles the SIMO spectrum, indicating low interference between transmitters. From this, it can be concluded that MIMO operation can happen with low interference between channels. Therefore NU-OTFS is a valid MIMO waveform when paired with the proposed low-complexity spectral division receiver.

B. Experimental Validation of OTFS Radar

In this section, experimental results of OTFS and NU-OTFS radar are presented. The data are gathered using the PARSAX radar [45]. Although PARSAX is a weather radar, it is programmed to send an OTFS frame to measure a static target at 1185 meters distance (Fig. 9). The OTFS waveform parameters are shown in Table II. A full OTFS frame is

TABLE II
OTFS MEASUREMENT WAVEFORM PARAMETERS

Parameter	Symbol	Value
Number of delay bins	N	1024
Number of Doppler bins	M	26
Bandwidth	B	40 MHz
Carrier frequency	f_c	3.315 GHz
Symbol duration	T	25.6 μs
Intercarrier separation	Δf	39.06 kHz
Cyclic prefix duration	T_{cp}	12.8 μs
Communication Modulation	$(-)$	QPSK

transmitted, and the sparse sampling in the time-frequency domain is performed digitally in the acquired signal. This approach serves to evaluate the radar performance of OTFS with experimental data for the first time, both with a full and sparse sampling of the time-frequency resources, while also allowing for the comparison of different multiplexing undersampling schemes.

In the measurements, we compare a fully sampled OTFS frame representing single-transmitter operation with frames with partial time-frequency sampling, simulating a single Tx channel in a MIMO system. For reference, we consider a system with four-channel multiplexing and thus the acquisition of 25% of samples of the full frame. First, we consider interleaved MIMO, where the transmitters are multiplexed through sequential allocation of time-frequency resources (labeled as sparse sequential), such as the example depicted in Fig. 2e. Furthermore, we consider a second approach where multiplexing is achieved through quasi-random sparse time-frequency allocation (labeled as sparse random), which is depicted in Fig. 2f and representative of NU-OTFS radar operation. Full frame estimation (100% sample acquisition) is used for reference. The estimation of radar parameters is performed using the same receiver as in the numerical validation in the previous section.

The DFT-based range estimation with the described sampling patterns is shown in Fig. 10, where the trade-off between sequential and arbitrary multiplexing in time-frequency can be clearly observed. Sequential sparse sampling of the time-frequency domain results in a dynamic range comparable to the fully sampled frame but a reduction in the unambiguous parameter estimation, as made clear by the appearance of a ghost target in the range domain. On the contrary,

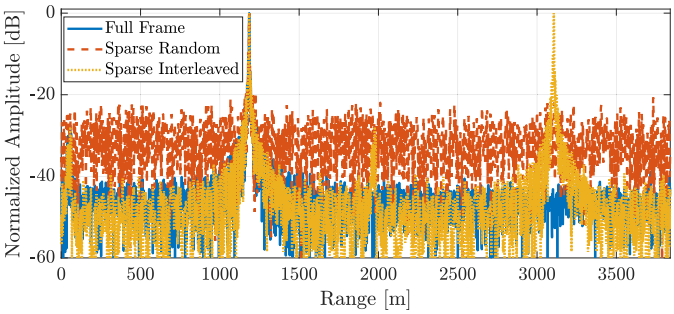

Fig. 10. Measured DFT-based range profile comparing a full OTFS single-transmitter frame with partially sampled frames for transmitter multiplexing. Sequential multiplexing reduces non-ambiguous parameter estimation, while NU-OTFS random multiplexing reduces the dynamic range.

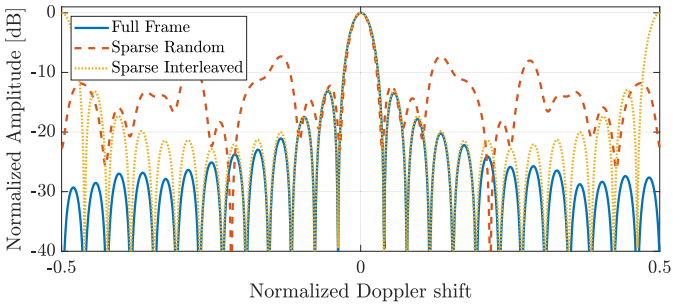

Fig. 11. Measured DFT-based Doppler profile comparing a full OTFS single-transmitter frame with sparse sampling for transmitter multiplexing.

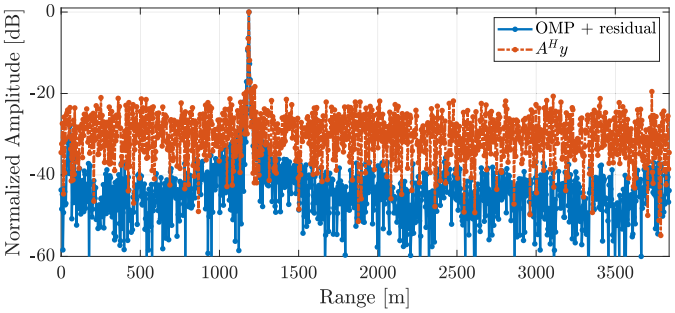

Fig. 12. Measured NU-OTFS range profile (sparse random) with standard DFT approach versus OMP-based reconstruction. OMP increases the dynamic range to levels comparable to full-frame measurements.

random sparse time-frequency patterns reduce the dynamic range under DFT processing but are able to achieve the same unambiguous parameter estimation as the single-transmitter signal. The same effect can be seen in the Doppler estimation shown in Fig. 7, where the sequential multiplexing MIMO waveform shows ambiguity at the end of the spectrum, whereas the random time-frequency multiplexing shows a reduction in the dynamic range of the estimation.

In section IV-A it was shown with simulations that sparse reconstruction algorithms (specifically, OMP) can help mitigate the dynamic range loss by using sparse sampling approaches. The results of applying OMP to the NU-OTFS waveform are shown in Fig. 12, where the DFT estimation of the randomly multiplexed NU-OTFS signal is compared to the output of OMP. It can be seen that by using OMP, the achieved dynamic range matches the noise floor in the full-frame estimation (Fig. 10). These experimental results show that NU-OTFS paired with sparse reconstruction algorithms can achieve comparable dynamic range to fully sampled OTFS

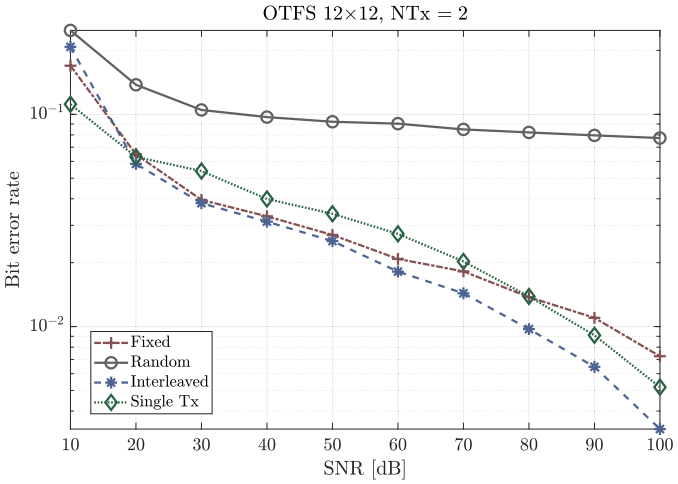

Fig. 13. Bit error rate for different values of SNR. Standard 3GPP EVA-2 channel used with nine taps and Rayleigh fading. UE speed is sampled for each tap from a uniform distribution between 0 and 100 kph.

frames while being able to multiplex multiple transmitters, thus validating the numerical results for NU-OTFS radar operation presented above.

C. MU Communication Performance Evaluation

To evaluate the communications performance of the proposed MU/MIMO approach, an LMMSE detector [42] is used for an OTFS communication frame propagating through a 3GPP standard *Extended Vehicular A* (EVA) [28] model channel with $n_{\text{taps}} = 9$, and complex gains h_i for $i \in \{1, \ldots, n_{\text{taps}}\}$ modeled as independent Rayleigh fading random variables. The Doppler associated to each tap is sampled from a uniform distribution of shifts in $[0\ \upsilon_{\max}]$, with

$$\upsilon_{max} = \frac{\Delta \mathrm{v}_{\max}}{c} f_0, \tag{33}$$

where $\mathrm{v}_{\max}$ is the maximum UE speed considered. Fig. 13 shows the bit error rate (BER) values for different subcarrier allocation patterns and increasing SNR values. The results are the average of 10000 Monte Carlo simulations with different noise, fading, and UE speed realizations ($\mathrm{v}_{\max} = 100$kph). The UE speed value for each Monte Carlo is sampled from a uniform $[0\ \mathrm{v}_{\max}]$ distribution. Random subcarrier allocation is compared to OTFS state-of-the-art interleaved allocation and single Tx performance with no multiplexing. Additionally, a stochastic search was used to find well-performing subcarrier allocation patterns in terms of BER. One of these selected patterns is used for comparison. In all cases, parameters are sampled from continuous distributions; therefore, off-grid error is present and uncompensated. For methods to mitigate the effects of off-grid error, see e.g. [46].

The simulations show that random subcarrier allocation results in a significant degradation in BER with respect to both the single user/SISO radar case and the state-of-the-art suggested interleaved subcarrier multiplexing. After closer inspection of the results, it is observed that the BER depends on the chosen subcarrier allocation pattern. Well-performing non-uniform subcarrier allocation patterns from the simulations are selected, and their performance is evaluated. It can

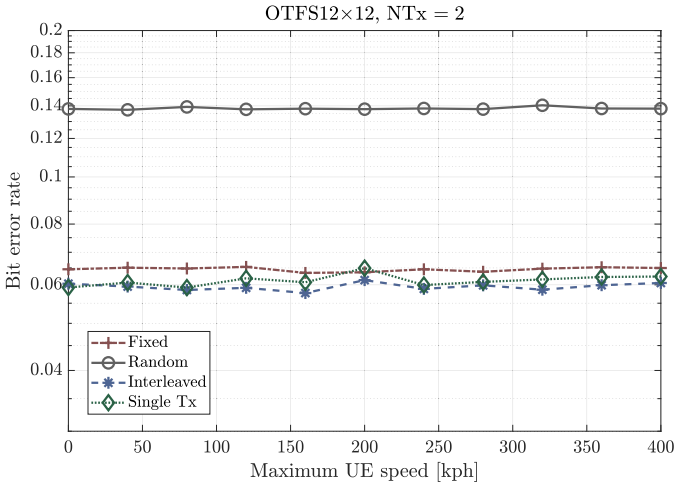

Fig. 14. Bit error rate versus different distributions of UE speed. Standard 3GPP EVA-2 channel with seven taps, Rayleigh fading, and SNR = 20 dB. UE speed is sampled for each tap from a uniform distribution between 0 and the maximum value.

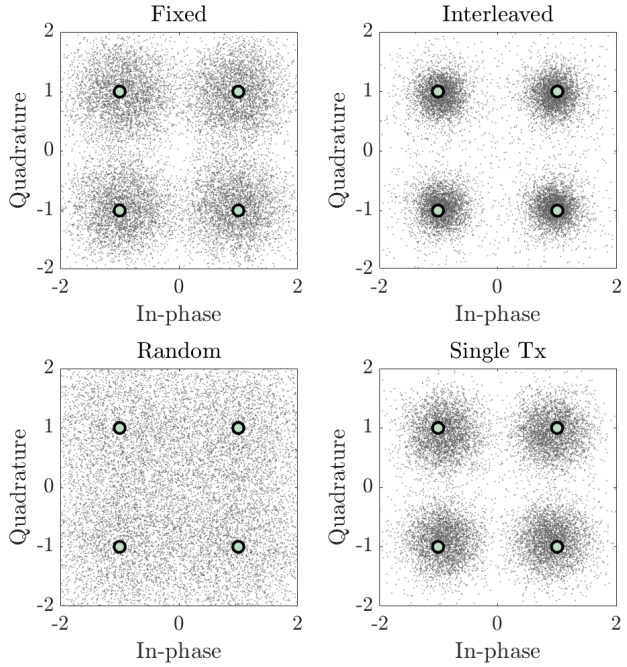

Fig. 15. IQ distribution of the recovered symbols after an LMSEE receiver in an EVA-2 channel with SNR of 20 dB and maximum UE speed of 100 kph.

be seen that the BER for realistic operating SNR values (i.e., in [15 40] dB [28]) of this pattern, labeled as *Fixed* in Fig. 13, closely matches the values of the interleaved pattern, only showing significant differences as SNR increases above realistic values. This validates the viability of the proposed NU-OTFS waveform for user multiplexing. The relatively high BER for all SNR values is attributed to a combination of realistic EVA-2 channel combined with unmitigated off-grid errors present in all simulations. Further study of the potential benefits of the added time-frequency allocation flexibility in NU-OTFS communications in partially interfered channels is left for future work, although similar approaches studied in the framework of cognitive radio have shown increased performance in comparable waveforms such as OFDM [47]. A comparison between the same set of patterns for increasing values of v_{max} is shown in Fig. 14, indicating that the chosen fixed subcarrier assignation pattern outperforms the random pattern, and maintains the Doppler tolerance of the interleaved and single-user/SISO radar case.

Fig. 15 shows the estimated received QPSK constellations for the same multiplexing patterns and channel conditions at SNR = 20dB, indicating that the interleaved-multiplexing constellation resembles the single-user closely. The QPSK received constellation using the Fixed distribution is more spread than the interleaved approach. Still, the symbols can be easily associated to each quadrant instead of the entirely random approach.

V. Conclusion

This article has investigated the problem of OTFS radcom under the requirement of non-uniform allocation of time-frequency resources for multiplexing in MU/MIMO applications. A novel OTFS-like waveform, NU-OTFS, is proposed to accomplish quasi-arbitrary time-frequency resource allocation, allowing for more flexible multiplexing schemes. NU-OTFS generalizes and extends previously proposed OTFS multiplexing strategies by using the NU-ISFFT to convert the delay-Doppler symbols into a non-uniform time-frequency frame. The performance of NU-OTFS in radar and communications has been evaluated through a combination of numerical simulations and radar measurements. Radar numerical and experimental data show that NU-OTFS allows for increased unambiguous Doppler and range estimations with a manageable side-lobe level when paired with hybrid 1D or 2D sparse estimation. For communications, numerical simulations of realistic vehicular channels show that although non-uniform sampling contributes to estimated symbol spread in the IQ representation, the BER performance in practical 5G/6G channel SNR resembles that of state-of-the-art MU configurations. Moreover, NU-OTFS shows the same performance in high-mobility scenarios as the interleaved and single-user full-frame approach. When considered jointly, these results suggest that NU-OTFS is a promising approach to OTFS Radcom, particularly when higher non-ambiguous parameter estimation is necessary for radar. Therefore, NU-OTFS is a viable alternative to standard OTFS when increased flexibility in time-frequency resource allocation is required for interference avoidance or increased radar performance.

Acknowledgment

The authors would like to thank Fred van der Zwan and Dr. Utku Kumbul for their support during the measurement campaigns.

References

[1] K. V. Mishra, M. R. B. Shankar, V. Koivunen, B. Ottersten, and S. A. Vorobyov, "Toward millimeter-wave joint radar communications: A signal processing perspective," *IEEE Signal Process. Mag.*, vol. 36, no. 5, pp. 100–114, Sep. 2019.

[2] A. Hassanien, M. G. Amin, Y. D. Zhang, and F. Ahmad, "Dual-function radar-communications: Information embedding using sidelobe control and waveform diversity," *IEEE Trans. Signal Process.*, vol. 64, no. 8, pp. 2168–2181, Apr. 2016.

[3] F. Liu, C. Masouros, A. Li, H. Sun, and L. Hanzo, "MU-MIMO communications with MIMO radar: From co-existence to joint transmission," *IEEE Trans. Wireless Commun.*, vol. 17, no. 4, pp. 2755–2770, Apr. 2018.
[4] J. Xu, X. Wang, E. Aboutanios, and G. Cui, "Hybrid index modulation for dual-functional radar communications systems," *IEEE Trans. Veh. Technol.*, vol. 72, no. 3, pp. 3186–3200, Mar. 2023.
[5] P. Kumari, S. A. Vorobyov, and R. W. Heath, "Adaptive virtual waveform design for millimeter-wave joint communication-radar," *IEEE Trans. Signal Process.*, vol. 68, pp. 715–730, 2020.
[6] B. Schweizer et al., "The fairy tale of simple all-digital radars: How to deal with 100 Gbit/s of a digital millimeter-wave MIMO radar on an FPGA [application notes]," *IEEE Microw. Mag.*, vol. 22, no. 7, pp. 66–76, Jul. 2021.
[7] G. Hakobyan and B. Yang, "High-performance automotive radar: A review of signal processing algorithms and modulation schemes," *IEEE Signal Process. Mag.*, vol. 36, no. 5, pp. 32–44, Sep. 2019.
[8] M. Bica and V. Koivunen, "Generalized multicarrier radar: Models and performance," *IEEE Trans. Signal Process.*, vol. 64, no. 17, pp. 4389–4402, Sep. 2016.
[9] M. F. Keskin, H. Wymeersch, and V. Koivunen, "MIMO-OFDM joint radar-communications: Is ICI friend or foe?" *IEEE J. Sel. Topics Signal Process.*, vol. 15, no. 6, pp. 1393–1408, Nov. 2021.
[10] R. Hadani et al., "Orthogonal time frequency space modulation," in *Proc. IEEE Wireless Commun. Netw. Conf. (WCNC)*, San Francisco, CA, USA, Mar. 2017, pp. 1–6.
[11] L. Gaudio, M. Kobayashi, G. Caire, and G. Colavolpe, "On the effectiveness of OTFS for joint radar parameter estimation and communication," *IEEE Trans. Wireless Commun.*, vol. 19, no. 9, pp. 5951–5965, Sep. 2020.
[12] T. M. C. Chu, H.-J. Zepernick, A. Westerhagen, A. Höök, and B. Granbom, "Performance assessment of OTFS modulation in high Doppler airborne communication networks," *Mobile Netw. Appl.*, vol. 27, no. 4, pp. 1746–1756, Feb. 2022, doi: 10.1007/s11036-022-01928-4.
[13] P. Raviteja, Y. Hong, E. Viterbo, and E. Biglieri, "Practical pulse-shaping waveforms for reduced-cyclic-prefix OTFS," *IEEE Trans. Veh. Technol.*, vol. 68, no. 1, pp. 957–961, Jan. 2019.
[14] G. D. Surabhi, R. M. Augustine, and A. Chockalingam, "Peak-to-average power ratio of OTFS modulation," *IEEE Commun. Lett.*, vol. 23, no. 6, pp. 999–1002, Jun. 2019.
[15] A. Correas-Serrano, N. Petrov, M. Gonzalez-Huici, and A. Yarovoy, "Comparison of radar receivers for OFDM and OTFS waveforms," in *Proc. 19th Eur. Radar Conf. (EuRAD)*, Sep. 2022, pp. 1–4.
[16] J. Li and P. Stoica, *MIMO Radar Signal Processing*. Hoboken, NJ, USA: Wiley, 2008.
[17] G. Babur, O. A. Krasnov, A. Yarovoy, and P. Aubry, "Nearly orthogonal waveforms for MIMO FMCW radar," *IEEE Trans. Aerosp. Electron. Syst.*, vol. 49, no. 3, pp. 1426–1437, Jul. 2013.
[18] H. Bolcskei, "MIMO-OFDM wireless systems: Basics, perspectives, and challenges," *IEEE Wireless Commun.*, vol. 13, no. 4, pp. 31–37, Aug. 2006.
[19] C. Sturm, Y. L. Sit, M. Braun, and T. Zwick, "Spectrally interleaved multi-carrier signals for radar network applications and multi-input multi-output radar," *IET Radar, Sonar Navigat.*, vol. 7, no. 3, pp. 261–269, Mar. 2013.
[20] L. Gaudio, M. Kobayashi, G. Caire, and G. Colavolpe, "Joint radar target detection and parameter estimation with MIMO OTFS," in *Proc. IEEE Radar Conf.*, Sep. 2020, pp. 1–6.
[21] Y. Ge, Q. Deng, P. C. Ching, and Z. Ding, "OTFS signaling for uplink NOMA of heterogeneous mobility users," *IEEE Trans. Commun.*, vol. 69, no. 5, pp. 3147–3161, May 2021.
[22] V. Khammammetti and S. K. Mohammed, "OTFS-based multiple-access in high Doppler and delay spread wireless channels," *IEEE Wireless Commun. Lett.*, vol. 8, no. 2, pp. 528–531, Apr. 2019.
[23] G. D. Surabhi, R. M. Augustine, and A. Chockalingam, "Multiple access in the delay-Doppler domain using OTFS modulation," 2019, *arXiv:1902.03415*.
[24] C. Knill, F. Roos, B. Schweizer, D. Schindler, and C. Waldschmidt, "Random multiplexing for an MIMO-OFDM radar with compressed sensing-based reconstruction," *IEEE Microw. Wireless Compon. Lett.*, vol. 29, no. 4, pp. 300–302, Apr. 2019.
[25] G. Hakobyan, M. Ulrich, and B. Yang, "OFDM-MIMO radar with optimized nonequidistant subcarrier interleaving," *IEEE Trans. Aerosp. Electron. Syst.*, vol. 56, no. 1, pp. 572–584, Feb. 2020.
[26] A. De Maio, Y. C. Eldar, and A. M. Haimovich, *Compressed Sensing in Radar Signal Processing*. Cambridge, U.K.: Cambridge Univ. Press, 2019.
[27] A. Correas-Serrano and M. A. Gonzalez-Huici, "Sparse reconstruction of chirplets for automotive FMCW radar interference mitigation," in *IEEE MTT-S Int. Microw. Symp. Dig.*, Apr. 2019, pp. 1–4.
[28] *Evolved Universal Terrestrial Radio Access (EUTRA); User Equipment (UE) Radio Transmission and Reception*, document TS 36.101, 3GPP, 2021. [Online]. Available: https://www.3gpp.org
[29] G. Babur, P. Aubry, and F. L. Chevalier, "Simple transmit diversity technique for phased array radar," *IET Radar, Sonar Navigat.*, vol. 10, no. 6, pp. 1046–1056, Jul. 2016.
[30] P. Raviteja, K. T. Phan, Y. Hong, and E. Viterbo, "Orthogonal time frequency space (OTFS) modulation based radar system," in *Proc. IEEE Radar Conf. (RadarConf)*, Apr. 2019, pp. 1–6.
[31] M. F. Keskin, H. Wymeersch, and A. Alvarado, "Radar sensing with OTFS: Embracing ISI and ICI to surpass the ambiguity barrier," 2021, *arXiv:2103.16162*.
[32] G. Hakobyan and B. Yang, "A novel intercarrier-interference free signal processing scheme for OFDM radar," *IEEE Trans. Veh. Technol.*, vol. 67, no. 6, pp. 5158–5167, Jun. 2018.
[33] C. Sturm, E. Pancera, T. Zwick, and W. Wiesbeck, "A novel approach to OFDM radar processing," in *Proc. IEEE Radar Conf.*, May 2009, pp. 1–4.
[34] J. H. G. Ender, "On compressive sensing applied to radar," *Signal Process.*, vol. 90, no. 5, pp. 1402–1414, May 2010.
[35] J. Wang, S. Kwon, and B. Shim, "Generalized orthogonal matching pursuit," *IEEE Trans. Signal Process.*, vol. 60, no. 12, pp. 6202–6216, Dec. 2012.
[36] A. Correas-Serrano and M. A. González-Huici, "Experimental evaluation of compressive sensing for DoA estimation in automotive radar," in *Proc. 19th Int. Radar Symp. (IRS)*, Jun. 2018, pp. 1–10.
[37] G. Hakobyan and B. Yang, "A novel OFDM-MIMO radar with non-equidistant subcarrier interleaving and compressed sensing," in *Proc. 17th Int. Radar Symp. (IRS)*, May 2016, pp. 1–5.
[38] A. Correas-Serrano et al., "Performance analysis and design of a distributed radar network for automotive application," in *Proc. 23rd Int. Radar Symp. (IRS)*, Sep. 2022, pp. 30–35.
[39] D. Mateos-Núñez, M. A. González-Huici, R. Simoni, F. B. Khalid, M. Eschbaumer, and A. Roger, "Sparse array design for automotive MIMO radar," in *Proc. 16th Eur. Radar Conf. (EuRAD)*, Oct. 2019, pp. 249–252.
[40] S. Tiwari, S. S. Das, and V. Rangamgari, "Low complexity LMMSE receiver for OTFS," *IEEE Commun. Lett.*, vol. 23, no. 12, pp. 2205–2209, Dec. 2019.
[41] P. Raviteja, E. Viterbo, and Y. Hong, "OTFS performance on static multipath channels," *IEEE Wireless Commun. Lett.*, vol. 8, no. 3, pp. 745–748, Jun. 2019.
[42] Y. Hong, T. Thaj, and E. Viterbo, *Delay-Doppler Communications: Principles and Applications*. Amsterdam, The Netherlands: Elsevier, 2022.
[43] R. Hadani and A. Monk, "OTFS: A new generation of modulation addressing the challenges of 5G," 2018, *arXiv:1802.02623*.
[44] M.-E. Chatzitheodoridi, A. Taylor, and O. Rabaste, "A mismatched filter for integrated sidelobe level minimization over a continuous Doppler shift interval," in *Proc. IEEE Radar Conf.*, Sep. 2020, pp. 1–6.
[45] O. A. Krasnov, G. P. Babur, Z. Wang, L. P. Ligthart, and F. van der Zwan, "Basics and first experiments demonstrating isolation improvements in the agile polarimetric FM-CW radar—PARSAX," *Int. J. Microw. Wireless Technol.*, vol. 2, nos. 3–4, pp. 419–428, Aug. 2010.
[46] Y. Ge, Q. Deng, P. C. Ching, and Z. Ding, "Receiver design for OTFS with a fractionally spaced sampling approach," *IEEE Trans. Wireless Commun.*, vol. 20, no. 7, pp. 4072–4086, Jul. 2021.
[47] J. Lunden, V. Koivunen, and H. V. Poor, "Spectrum exploration and exploitation for cognitive radio: Recent advances," *IEEE Signal Process. Mag.*, vol. 32, no. 3, pp. 123–140, May 2015.

Aitor Correas-Serrano received the B.Sc. and M.Sc. degrees in telecommunications engineering from the Technical University of Cartagena in 2015 and 2017, respectively. During his master's program, he worked as a Research Engineer at the Fraunhofer Institute for high-frequency physics and radar (FHR), Wachtberg, Germany, where he researched Compressed Sensing methods applied to automotive radar. Since 2017, he has been a Research Associate with the Fraunhofer FHR, where he continued his work on radar technologies. Since January 2020, he has been also a Ph.D. candidate as part of the Microwave Sensing, Signals and Systems group at TU Delft. His main research interests include compressed sensing, MIMO waveform design, interference cancellation, and adaptive strategies for multifunctional radar and communication systems.

Nikita Petrov received the Engineering degree in radio-electronic control systems from Baltic State Technical University Voenmeh, Saint Petersburg, Russia, in 2012, and the Ph.D. degree in radar signal processing from the Delft University of Technology, Delft, The Netherlands, in 2019.

Since 2019, he has been a Post-Doctoral Researcher with the Microwave Sensing, Signals and Systems (MS3) Section, Faculty of Electrical Engineering, Mathematics, and Computer Science (EEMCS), Delft University of Technology. Since April 2022, he has been a principal radar signal processing engineer at NXP Semiconductors N.V., Eindhoven, The Netherlands, and he holds an advisory position in the same group at the Delft University of Technology. His research interests include modern radar technologies, radar signal processing, multichannel and multiband signals and systems, and high-resolution and automotive radars.

Dr. Petrov serves as a Reviewer for a few IEEE TRANSACTIONS AND RADAR CONFERENCES.

Maria Gonzalez-Huici received the diploma degree in theoretical physics from the Autonoma University of Madrid in September 2002, followed by 2 years of postgraduate studies in particle physics and astrophysics from the University of Bonn, and the Ph.D. degree in physics from the University of Bonn in 2013, on the topic of detection and classification of buried landmines with radar. Since May 2005, she has been working as a Research Associate at Fraunhofer FHR. Since 2015, she has been leading the Adaptive Perception team at FHR. Since April 2023, she has also been leading Signal Processing and Algorithms Department. Her research focuses on MIMO radar, signal and array processing, waveform design, compressed sensing, deep learning, and sensor data fusion.

Alexander Yarovoy (Fellow, IEEE) received the diploma degree (Hons.) in radiophysics and electronics and the Physics and Mathematics Science and Doctor Physics and Mathematics Science degrees in radiophysics from the Kharkov State University, Ukraine, in 1984, 1987, and 1994, respectively. In 1987 he joined the Department of Radiophysics, Kharkov State University, as a Researcher and became a Full Professor in 1997. From September 1994 to 1996, he was with the Technical University of Ilmenau, Germany, as a Visiting Researcher. Since 1999, he has been with the Delft University of Technology, the Netherlands. Since 2009 he has been leads there a chair of Microwave Sensing, Systems and Signals. He has authored and co-authored more than 550 scientific or technical papers, seven patents and fourteen book chapters. His main research interests are in high-resolution radar, microwave imaging and applied electromagnetics (in particular, UWB antennas). He is the recipient of the European Microwave Week Radar Award for the paper that best advances the state-of-the-art in radar technology in 2001 (together with L.P. Ligthart and P. van Genderen) and in 2012 (together with T. Savelyev). In 2023 together with Dr. I.Ullmann, N. Kruse, R. Gündel and Dr. F. Fioranelli he got the best paper award at IEEE Sensor Conference. In 2010 together with D. Caratelli he got the best paper award of the Applied Computational Electromagnetic Society (ACES). He served as the General TPC chair of the 2020 European Microwave Week (EuMW'20), as the Chair and TPC chair of the 5th European Radar Conference (EuRAD'08), as well as the Secretary of the 1st European Radar Conference (EuRAD'04). He served also as the co-chair and TPC chair of the Xth International Conference on GPR (GPR2004). He serves as an Associated Editor of the IEEE TRANSACTION ON RADAR SYSTEMS. From 2011 to 2018, he served as an Associated Editor of the *International Journal of Microwave and Wireless Technologies*. In the period 2008 to 2017, he served as the Director of the European Microwave Association (EuMA).